Thermonuclear reaction ^{30}S(p,γ)^{31}Cl studied via Coulomb breakup of ^{31}Cl

C. Langer,[1,2,*,†] O. Lepyoshkina,[3] Y. Aksyutina,[2] T. Aumann,[2,4] S. Beceiro Novo,[5,†] J. Benlliure,[5] K. Boretzky,[2] M. Chartier,[6] D. Cortina,[5] U. Datta Pramanik,[7] O. Ershova,[1,2] H. Geissel,[2] R. Gernhäuser,[3] M. Heil,[2] G. Ickert,[2] H. T. Johansson,[2,8] B. Jonson,[8] A. Kelić-Heil,[2] A. Klimkiewicz,[2,9] J. V. Kratz,[10] R. Krücken,[3,11] R. Kulessa,[9] K. Larsson,[2] T. Le Bleis,[1,2,12] R. Lemmon,[13] K. Mahata,[2] J. Marganiec,[2,14] T. Nilsson,[8] V. Panin,[2,4] R. Plag,[1,2] W. Prokopowicz,[2] R. Reifarth,[1,2,‡] V. Ricciardi,[2] D. M. Rossi,[2,10,†] S. Schwertel,[3] H. Simon,[2] K. Sümmerer,[2] B. Streicher,[2] J. Taylor,[6] J. R. Vignote,[2] F. Wamers,[2,4] C. Wimmer,[1,2] and P. Z. Wu[6]

[1]*Goethe-Universität Frankfurt am Main, Max-von-Laue-Str. 1, D-60438 Frankfurt am Main, Germany*
[2]*GSI Helmholtzzentrum für Schwerionenforschung GmbH, D-64291 Darmstadt, Germany*
[3]*Physik-Department E12, Technische Universität München, D-85748 Garching, Germany*
[4]*Institut für Kernphysik, Technische Universität Darmstadt, D-64289 Darmstadt, Germany*
[5]*University of Santiago de Compostela, E-15782 Santiago de Compostela, Spain*
[6]*University of Liverpool, Liverpool L69 7ZE, United Kingdom*
[7]*SINP, Kolkata 700-064, India*
[8]*Chalmers University of Technology, SE-41296 Göteborg, Sweden*
[9]*Jagiellonian University, PL-30-059 Krakow, Poland*
[10]*Institut für Kernchemie, Johannes Gutenberg-Universität, D-55128 Mainz, Germany*
[11]*TRIUMF, Vancouver, British Columbia V6T 2A3, Canada*
[12]*IPHC, F-67037 Strasbourg, France*
[13]*STFC Daresbury Laboratory, Warrington WA4 4AD, United Kingdom*
[14]*ExtreMe Matter Institute EMMI and Research Division, GSI, Darmstadt, Germany*

(Received 11 November 2013; published 20 March 2014)

Coulomb breakup at high energy in inverse kinematics of proton-rich ^{31}Cl was used to constrain the thermonuclear ^{30}S$(p,\gamma)^{31}$Cl capture reaction rate under typical Type I x-ray burst conditions. This reaction is a bottleneck during rapid proton-capture nucleosynthesis (rp process), where its rate depends predominantly on the nuclear structure of ^{31}Cl. Two low-lying states just above the proton-separation threshold of $S_p = 296(50)$ keV in ^{31}Cl have been identified experimentally using the R^{3}B-LAND setup at the GSI Helmholtzzentrum für Schwerionenforschung GmbH. Both states are considered to play a key role in the thermonuclear ^{30}S$(p,\gamma)^{31}$Cl capture reaction. Excitation energies of the first $J^\pi = 1/2^+,5/2^+$ states have been extracted and the reaction rate for proton capture on ^{30}S under typical rp-process temperatures has been investigated.

DOI: 10.1103/PhysRevC.89.035806 PACS number(s): 25.70.De, 21.60.Cs, 26.30.Ca, 29.38.Db

I. INTRODUCTION

Astrophysical Type I x-ray bursts are powerful recurring thermonuclear explosions, ignited in the envelope of a compact and dense neutron star in a low-mass x-ray binary system. In this system, a relatively unevolved star orbits the neutron star which accretes H/He-rich matter from the companion star onto an accretion disk formed around the neutron star. During accretion, the matter is heated and compressed, and, eventually, a thermonuclear explosion is ignited.

The main energy generation is driven by a series of proton-capture reactions and corresponding β^+ decays and electron-capture reactions, also known as the rapid proton-capture process (rp process). This hydrogen burning process consumes the accreted protons in fast (p,γ) reactions, quickly synthesizing elements up to the proton-rich $A \approx 100$ region in only 10–100 s, see, e.g., [1–4].

The energy generated can be observed as a peak in the luminosity curve in the x-ray continuum. Lots of observational data have been accumulated in the past 15 years and can be used to validate Type I x-ray burst models [5]. Accurate input parameters determined mainly by the nuclear properties of the involved nuclei are of utmost importance for detailed network calculations. These properties, however, are difficult to obtain experimentally, since the rp-process path lies along the proton dripline [6], and experiments remain extremely challenging in this region.

Reaction rates for (p,γ), (α,p), and (α,γ) reactions are key input parameters for accurate nucleosynthesis calculations. Under certain conditions, reaction rates can be obtained from statistical-model calculations; such calculations are not applicable, however, in cases where single resonances dominate the reaction rate. Similarly, shell-model calculations can be used to derive structural information for certain identified nuclei [7]. However, the calculations usually exhibit large errors up to hundreds of keV for the excitation energies, and thus uncertainties of several orders of magnitude in the reaction rate are introduced.

Certain nuclei on the rp-process path are called *waiting points* since the reaction flow is supposed to be halted at

*c.langer@gsi.de
†Present address: National Superconducting Cyclotron Laboratory, Michigan State University, East Lansing, MI 48824, USA.
‡reifarth@physik.uni-frankfurt.de

these nuclei until β decay has occurred. The $A = 30$ sulfur isotope with 16 protons and 14 neutrons is considered to be such a waiting point: The Q value for the ^{30}S$(p,\gamma)^{31}$Cl reaction is relatively small with $Q = 296(50)$ keV [8], and, consequently, a (p,γ)-(γ,p) equilibrium develops such that matter is accumulated at ^{30}S. In principle, the reaction ^{30}S$(\alpha,p)^{33}$Cl could serve as a bypass of the waiting point, but its rate is still highly uncertain and only recently a first measurement of the time-reversed reaction, still measured above the typical energies for Type I x-ray bursts, became possible at the ATLAS facility [9].

Consequently, β^+ decay to ^{30}P is assumed to be the next step on the rp-process path. Under typical x-ray burst conditions ($T_9 = 1$ GK, $\rho_{\max} = 10^6$ g/cm^3) the β^+ decay half-life of ^{30}S is $t_{1/2} \approx 1.06$ s [terrestrial $t_{1/2} = 1.178(5)$ s] [10] and is thus relatively long compared to the timescale of the full rp process (10–100 s). Depending strongly on the excitation energies of low-lying levels in ^{31}Cl, the ^{30}S(p,γ) reaction may serve as a possible bypass of the relatively long ^{30}S β^+ decay. To put these arguments on a firm experimental basis, it is of crucial importance to obtain spectroscopic information on the low-lying level structure of ^{31}Cl.

So far, only scarce experimental information on the level structure of ^{31}Cl is available. In an ^{31}Ar β-delayed two-proton emission experiment at ISOLDE [11], the authors observed a weak feeding of a 750 keV level in ^{31}Cl, which exhibits, however, forbidden decay character, and is thus excluded from their evaluation of β strength. In principle, the observed peak in this experiment could also arise from the β-delayed two-proton emission from ^{31}Ar, instead of the one-proton emission. However, in a subsequent compilation by the same group, the β-delayed two-proton decay of ^{31}Ar was studied again [12], but the weak feeding of the previously observed 750 keV state in ^{31}Cl was not discussed and left uncertain. A second excited state was observed in the same experiment on the ^{31}Ar β-delayed two-proton emission [11], and was later confirmed in [12]. This state has an excitation energy of $\sim$1750 keV.

In a recent work by Wrede *et al.* [13], the authors used the isobaric multiplet mass equation (IMME) to derive the low-lying level structure of ^{31}Cl. They incorporated updated experimental information on energies and masses for corresponding analog states in the isobars along the ($T = 3/2$, $A = 31$) multiplet in the IMME calculation and extracted the excitation energy of the astrophysically important first low-lying excited state in ^{31}Cl. According to Wrede *et al.*, the first excited state in ^{31}Cl is a $J^\pi = 1/2^+$ state with an energy of $\sim$745 keV, thus supporting the, so far uncertain, observation of this state in [11]. However, the authors based the calculation for this state on a *tentative* $T = 3/2$ assignment for ^{31}S, and, thus, along with Iliadis *et al.* [14], they stress the importance of an independent measurement of the resonance structure of ^{31}Cl. Especially an unambiguous experimental confirmation and extraction of the excitation energy of the lowest resonance situated just above the proton-separation threshold is still missing and of utmost importance in order to constrain the proton-capture reaction rate on ^{30}S.

Coulomb-breakup experiments offer a powerful tool to extract astrophysically important properties for very short-lived nuclei, like, e.g., spectroscopic information and radiative-capture cross sections via detailed balance [15–20]. Therefore, a Coulomb-breakup experiment of proton-rich nuclei in the intermediate-mass region was performed which was related to two different subjects: Nuclear Astrophysics (^{31}Cl) and Nuclear Structure Physics (possible appearance of low-lying dipole strength in proton-rich ^{32,34}Ar, see, e.g., [21]). In this work we present the result related to Nuclear Astrophysics, i.e., the Coulomb breakup of ^{31}Cl.

For the first time, both low-lying resonances in ^{31}Cl have been identified unambiguously, allowing experimental confirmation of the astrophysically important first excited state in ^{31}Cl. We discuss in Sec. II of the present paper the experiment and parts of the analysis. Section III presents the result of the measurement. Finally, in Sec. IV, the results will be discussed in terms of implications on the astrophysical capture-reaction rate. In addition, the newly derived reaction rate will be compared to the commonly used reaction rate from Wrede *et al.* (for a compilation of available rates see, e.g., the REACLIB compilation [22]).

II. THE EXPERIMENT

In order to extract spectroscopic information for the low-lying proton-decaying states in ^{31}Cl, the experiment was performed at the GSI Helmholtzzentrum für Schwerionenforschung GmbH in Darmstadt, employing the R^{3}B-LAND setup for measurements in inverse and full kinematics [23]. A sketch of the setup is shown in Fig. 1. The setup comprises various detector types, in order to identify and reconstruct the four-momentum of each individual particle on an event-by-event basis.

To produce the ^{31}Cl secondary beam at relativistic beam energies via the in-flight fragmentation method, an ^{36}Ar primary beam at 825A MeV impinged on a 6.347 g/cm^2 Be target, situated at the entrance of the fragment separator (FRS) [24].

The radioactive isotope ^{31}Cl ($t_{1/2} = 150$ ms) was subsequently selected via the $B\rho$-ΔE-$B\rho$ technique in the FRS and finally transported to the experimental setup at a beam energy of around 650A MeV. Isotopes with similar mass-over-charge ratios, however, were also delivered to the experimental setup due to the finite momentum acceptance of the FRS. Using the clear separation of the delivered isotopes, Coulomb-breakup studies on different isotopes in this mass region are possible.

The isotopes in the mixed beam were uniquely identified by means of time-of-flight and energy-loss measurements (Fig. 2). Absolute calibrations were performed by utilizing energy-loss and time-of-flight measurements with beams at known energies in combination with the ATIMA package for calibration of the energy loss in the detector material [25]. In order to focus on reactions with ^{31}Cl only, a two-dimensional gate was used to select the desired isotope in the incoming channel.

The mixed radioactive beam was directed onto the secondary reaction target, which was situated at the center of a 4π NaI γ-ray detector, consisting of 162 NaI crystals used to measure de-excitation γ rays of the reaction residues [26]. Calibration sources (^{22}Na, ^{60}Co, ^{88}Y) were used to calibrate

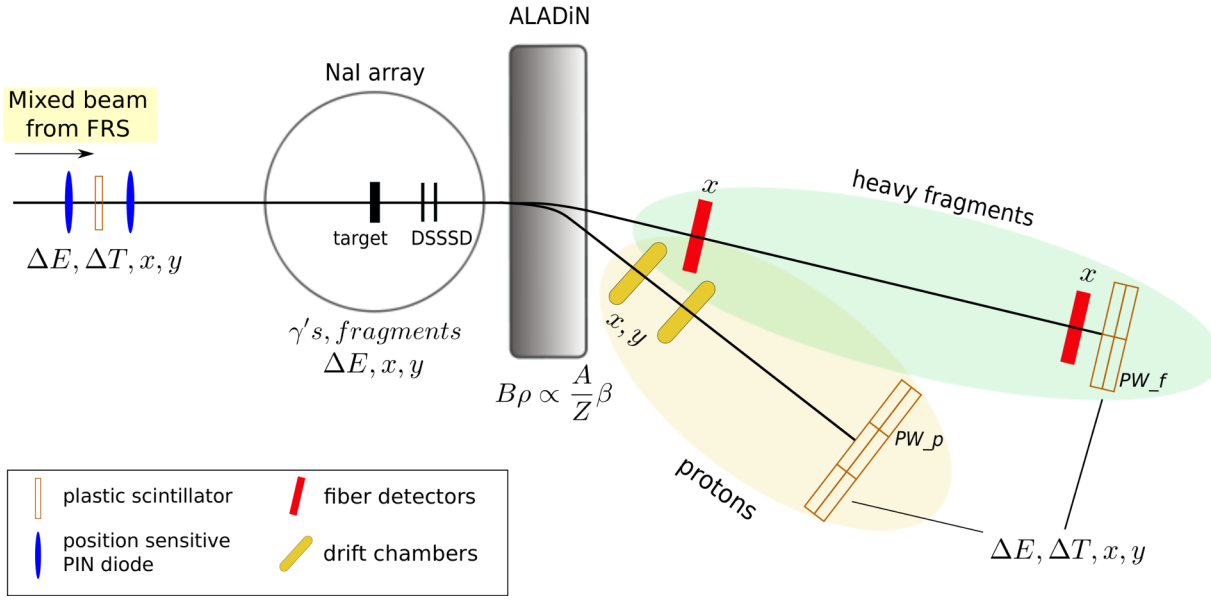

FIG. 1. (Color online) Schematic view of the R^{3}B-LAND setup used for the present experiment (not to scale). The mixed radioactive beam from the FRS enters the setup from the left-hand side of the figure. The physical quantities measured with various detectors are indicated in the figure. See text for more details.

the reconstructed energy of the γ rays. Moreover, a PuC source ($E_\gamma = 6.13$ MeV) was used for calibration of the high-energy range.

In order to induce electromagnetic excitations, a $^{\text{nat}}$Pb target with an areal density of 515 mg/cm^2 was used. Besides the measurement performed with the $^{\text{nat}}$Pb target, several runs without an inserted target were used to accurately subtract the background contributions stemming from secondary reactions in different detectors and parts of the beam line. In order to properly disentangle nuclear contributions and electromagnetically induced excitations, measurements with a ^{12}C target with an areal density of 369.8 mg/cm^2 were also performed. Downstream from the secondary reaction target, two arrays of double-sided Si microstrip detectors (DSSSDs) were placed to measure the interaction positions and the energy loss of the heavy residue and the protons (similar to the detectors in [27]).

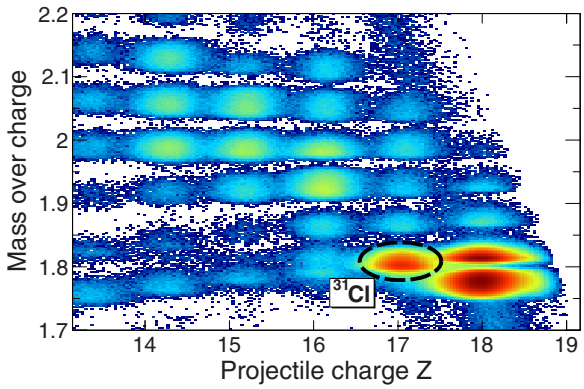

FIG. 2. (Color online) Incoming particle identification derived from magnetic-rigidity, time-of-flight, and energy-loss measurements. The color scale is logarithmic.

The magnetic field of a large dipole magnet (ALADIN) was used to separate the reaction products according to their magnetic rigidity. In the final stage of the setup, the hit position and time-of-flight of every heavy ion and proton was measured to reconstruct the exact trajectory and to derive the four-momentum of each particle. In order to achieve sufficient position resolution ($\approx$ 1 mm given by the fiber width) for the reconstruction of the trajectory of the heavy ions, large-area scintillation fiber detectors were used [28,29]. For the proton hit detection, multiwire proton drift chambers were placed behind the ALADIN magnet, achieving sub-millimeter spatial resolution. A dedicated tracking algorithm was developed, which accurately reconstructs the trajectory of each particle from the reaction vertex in the target to the final interaction position.

Figure 3 shows the identification of different reaction products via energy-loss measurements directly behind the target in the Si strip detectors (DSSSDs) and in the plastic-scintillator wall (PW_f) at the end of the setup. Several reaction products can be clearly identified. While the beam passes through different detectors and beam line materials, break-up reactions occur and need to be distinguished from real reactions induced in the secondary reaction target (see caption of Fig. 3 for further explanation). In combination with the mass reconstruction provided by the tracking algorithm, a two-dimensional gate is used to select the corresponding reaction channel ^{31}Cl(γ^*,p)^{30}S (where γ^* denotes the virtual character of the photon).

In order to extract spectroscopic information from the measured data, the invariant-mass technique is used. In this approach, the four-momenta of all reaction products from the decay of the excited continuum states are related to the energy

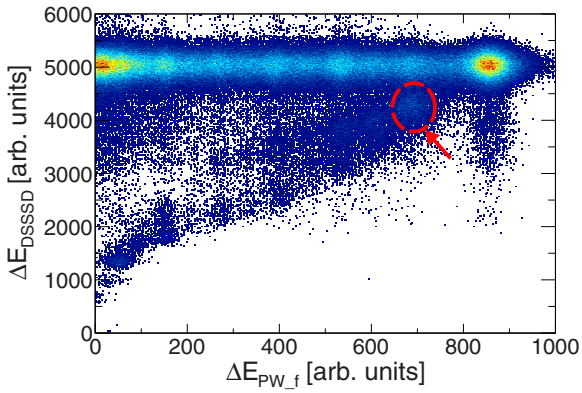

FIG. 3. (Color online) Energy loss measured in the double-sided Si microstrip detector (DSSSD) behind the Pb target plotted versus the one measured in the plastic wall PW_f at the end of the fragment trajectory. The horizontal ridge at ordinate values of 5000 units corresponds to beam particles that do not react in the Pb target, but that may lose one or more protons further downstream. The oval marks events considered in the reaction channel. The color scale is linear.

of the incoming ion, forming a Lorentz-invariant quantity. Using the masses m_i of ^{31}Cl, m_f for ^{30}S, and the proton mass m_p, the excitation energy E^* of ^{31}Cl can be reconstructed via

$$E^* = \sqrt{m_f^2 + \gamma_f \gamma_p m_f m_p (1 - \beta_f \beta_p \cos \Theta_{fp})} + E_\gamma - m_i, \tag{1}$$

with $\gamma_{f,p}$ being the Lorentz factor for the heavy residue and the proton, $\beta_{f,p}$ the velocities, the angle between the proton and the heavy residue Θ_{fp}, and the γ-ray energy E_γ for de-excitation γ rays of ^{30}S. The velocities were measured by time-of-flight, the scattering angle was extracted with the tracking algorithm and the γ-ray transitions were measured with the array of NaI crystals.

The opening angle of the beam line downstream from the target is ∼80 mrad. Hence, the data need to be corrected for possible acceptance cuts along the beam line. In order to yield a realistic acceptance correction, the simulation package R3BROOT, which is incorporated into the FAIRROOT package [30], was employed. It contains full geometrical information about the setup and it can be used to simulate fragment and proton tracks through the setup. A simple event generator was utilized to produce proton and fragment events. GEANT3 and GEANT4 transport engines were used to simulate the penetration of the particles through the different materials. It turns out, that up to an excitation energy of ∼4 MeV, the acceptance of the setup for this experiment was approximately 100%.

In addition, the intrinsic efficiency of the proton detection in the drift chambers and the plastic wall PW_p was determined by analyzing coincidences between the various detectors. The intrinsic one-proton detection efficiency of the proton branch was determined to be 63(8)%, the error being purely statistical.

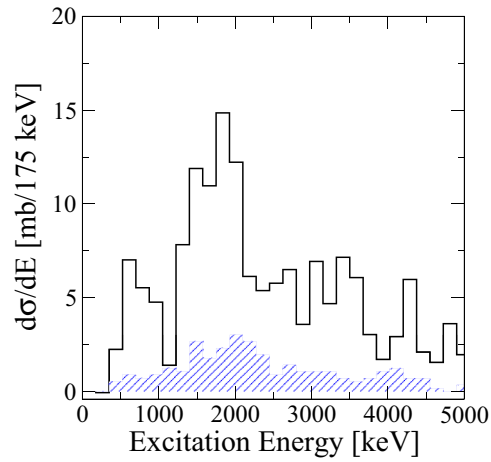

FIG. 4. (Color online) Energy-differential excitation spectrum derived after subtracting contributions from background. The shaded area corresponds to the part stemming from nuclear contributions. See text for details.

III. RESULTS

In order to treat background contributions properly, data taken without a target were subtracted from the dataset. Data taken with the ^{12}C target were used to disentangle nuclear contributions from the electromagnetic excitations induced in the ^{nat}Pb target and were subsequently also subtracted from the dataset (see [31] for a detailed description). The nuclear contribution, however, was relatively small (around 15%) and a safe subtraction was therefore possible (Fig. 4).

To account for feeding of excited states in the heavy-residual nucleus ^{30}S, de-excitation γ rays were detected with the NaI crystal array. An event-by-event Doppler-corrected γ-ray sum spectrum up to 5 MeV is shown in Fig. 5 under the condition that a Coulomb excitation and subsequent breakup

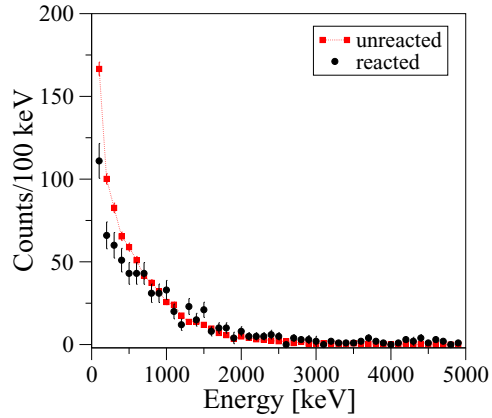

FIG. 5. (Color online) Doppler-corrected γ-ray sum spectrum in the case of incoming ^{31}Cl, with a subsequent reaction to ^{30}S (black circles). The background (red squares) is taken from unreacted beam in the outgoing channel normalized to the same number of incoming ions. The γ-ray sum spectrum shows no significant contribution from any excited state fed in the ^{30}S ejectile nucleus after the proton emission of ^{31}Cl*.

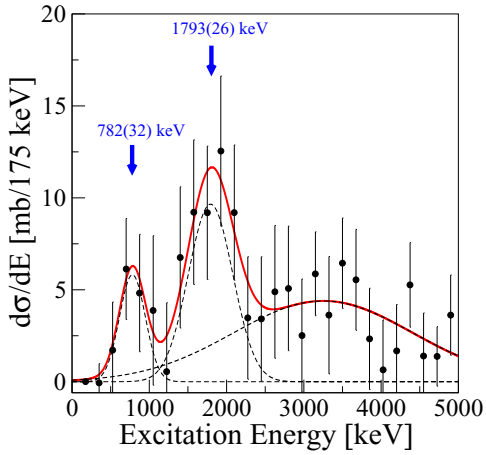

FIG. 6. (Color online) Energy-differential excitation spectrum of ^{31}Cl after subtraction of nuclear contributions. A fit, composed of three single Gaussians, is fitted to the data showing two low-lying resonance structures below 2 MeV (red solid line). The dashed lines correspond to the single contributions of the fit. See text for details.

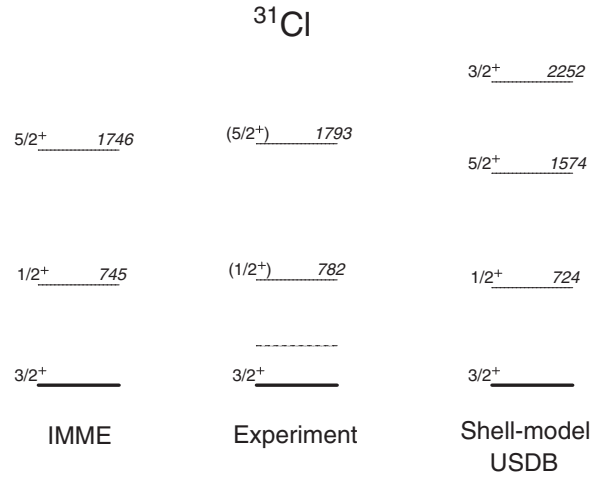

FIG. 7. Extracted level scheme for ^{31}Cl compared to the IMME calculation of Wrede *et al.* [13] and a shell-model calculation utilizing the USDB Hamiltonian [33]. The proton separation energy of 296 keV is indicated by the dashed line. Spin-parity assignments are solely based on the theoretical calculations. Energies are given in keV. See Table I and text for more details.

of ^{31}Cl to ^{30}S occurred in the target. For comparison, the normalized γ-ray sum spectrum in coincidence with unreacted ^{31}Cl in the final state is also shown. In this case, detected γ-ray events are mainly due to atomic processes occurring in the relatively thick $^{\text{nat}}$Pb target during the passage of the beam through the target.

As can be clearly seen in Fig. 5, no de-excitation γ rays can be identified above the atomic background, and, thus, no excited states in ^{30}S were populated after the decay of ^{31}Cl (the first excited 2^+ state in ^{30}S is located at $E_x = 2210.6(5)$ keV [32]). In this case, the E_γ term in Eq. (1) vanishes.

Figure 6 shows the background-subtracted energy-differential excitation spectrum for ^{31}Cl for pure electromagnetic excitations. Three different enhanced structures are visible. Below an excitation energy of 2 MeV, two resonant structures can be identified. A Gaussian fit was used to extract the excitation energies for the two excited low-lying states (since the width of the peaks is dominated by the resolution of the setup). At higher energies, a broad Gaussian function was fitted to the data to account for possible high-lying and nonresonant contributions. The overall fit describes the data well and the resonance energies are extracted from the fits. A peak at an excitation energy of $E_x = 782(32)$ keV is observed. Moreover, an excitation energy of $E_x = 1793(26)$ keV is extracted for the second low-lying resonance. The errors are dominated by statistics.

The results are in good agreement with predictions for ^{31}Cl. Figure 7 shows the extracted level scheme for ^{31}Cl in comparison with the IMME calculation [13] and a shell-model calculation, employing the USDB Hamiltonian, specifically suited for intermediate-mass *sd*-shell nuclei [33]. The shell-model calculation was carried out using the code NUSHELLX@MSU [34]. Our experiment clearly was not able to determine the spins and parities of the resonances in ^{31}Cl. However, the shell-model calculation and the analysis of isobaric analog states along the ($T = 3/2$, $A = 31$) multiplet suggests the spin-parity assignment as shown in parentheses in Fig. 7. Table I summarizes the extracted excitation energies and the resonance parameters used to calculate the reaction rate for the ^{30}S(p,γ)^{31}Cl reaction in Sec. IV.

IV. REACTION RATE

If a radiative proton-capture reaction proceeds through narrow resonances r, the resonant reaction rate can be calculated by

$$N_A\langle\sigma v\rangle = 1.54\times10^{11}(\mu T_9)^{-3/2}\sum_r(\omega\gamma)_r \times e^{-11.605E_r/k_BT_9}\ [\text{cm}^3\text{s}^{-1}\text{mole}^{-1}], \quad (2)$$

with N_A being the Avogadro number, μ the reduced mass, T_9 the temperature in GK, k_B the Boltzmann constant, and E_r the resonance energy, see, e.g., [35]. Besides the resonance energy, the strength of the resonance, denoted with $\omega\gamma$ in Eq. (2), is important in the calculation. It is related to the partial and total

TABLE I. Excitation energies E_x of ^{31}Cl extracted in this work and the resonance energies E_r in the c.m. system for ^{30}S(p,γ)^{31}Cl compared to the results from Wrede *et al.* [13]. Moreover, the partial γ-width is shown (taken from [13]), which is used to calculate the reaction rate in Sec. IV. The Q value for the reaction ^{30}S(p,γ)^{31}Cl of 296(50) keV [8] is used for the present work.

J^π	E_x (keV)	E_r (keV)	Γ_γ (meV)	Reference
$(1/2^+)$	782(32)	486(59)	$0.86^{+0.60}_{-0.35}$	This work
$1/2^+$	745(16)	461(15)		Wrede *et al.* [13]
$(5/2^+)$	1793(26)	1497(56)	$0.80^{+0.56}_{-0.33}$	This work
$5/2^+$	1746(7)	1462(5)		Wrede *et al.* [13]

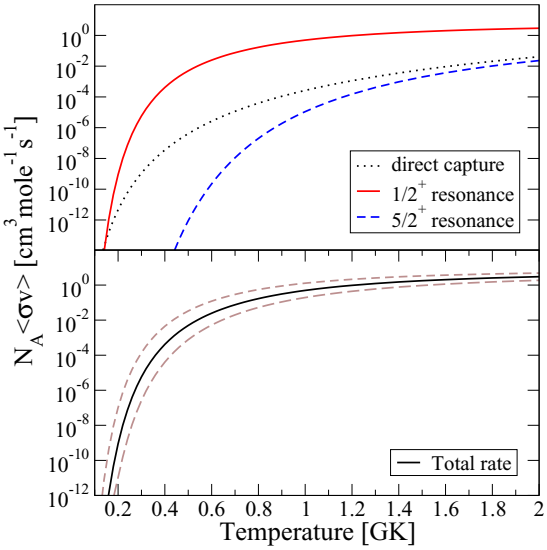

FIG. 8. (Color online) The calculated reaction rate for ^{30}S$(p,\gamma)^{31}$Cl. Top: The individual contributions are shown. Proton capture into the first excited state is the dominant contribution. Bottom: Total reaction rate (solid line) with error bands (dashed line).

width of the resonance and a statistical factor:

$$\omega\gamma = \frac{(2J_r+1)}{(2J_p+1)(2J_S+1)}\left(\frac{\Gamma_p\Gamma_\gamma}{\Gamma}\right). \quad (3)$$

Here, J_p, J_r, and J_S are the spins of the proton, of the resonance and of ^{30}S(g.s.). Furthermore, the sum of the partial proton-width Γ_p and the partial γ-width Γ_γ yields the total width $\Gamma = \Gamma_p + \Gamma_\gamma$. Since $\Gamma_p \gg \Gamma_\gamma$ for a narrow, mainly proton-decaying resonance, the total resonance strength Γ is dominated by the partial proton-width Γ_p. This reduces the resonance strength to $\omega\Gamma_\gamma$. Assuming isospin symmetry, the partial γ-width Γ_γ can be determined from the lifetime of analog isospin mirror states in ^{31}Si [13].

In addition, the direct-capture component to the reaction rate was taken into account. The astrophysical S_0 factor from [36] was used for this particular reaction and is 5.14×10^{-3} MeV b.

Finally, the total reaction rate is the sum of the different resonance contributions and the non-resonant part. The top panel of Fig. 8 shows the individual contributions to the reaction rate, whereas the bottom part shows the total proton-capture rate for the ^{30}S$(p,\gamma)^{31}$Cl reaction under typical Type I x-ray burst conditions.

In order to evaluate the reaction rate used in compilations, the ratio of the rate by Wrede *et al.* and the rate determined in this work is shown in Fig. 9 for temperatures between $T_9 = 0.1$ and 2 GK. In general, the rate is dominated by the contribution from the first excited state in ^{31}Cl. At temperatures below 0.15 GK, the direct-capture component is becoming dominant, which can be seen in Fig. 9, where the reaction-rate ratio approaches unity (since the same S_0 factor is used). At higher temperatures, the energy difference in the first excited state from the IMME calculation and the experimental data

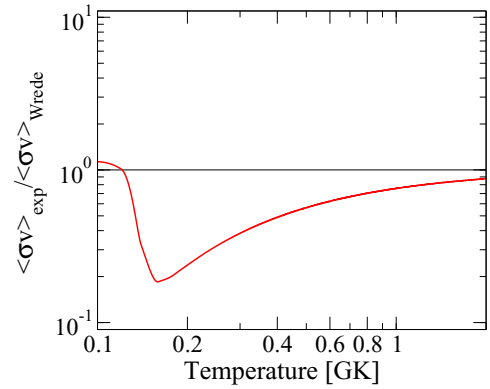

FIG. 9. (Color online) Reaction-rate ratio of the rate extracted with the IMME by Wrede *et al.* [13] and the present work. The deviation in the energy of the first excited state in ^{31}Cl between the IMME calculation and the experimental data leads dominantly to the rate differences in the temperature range below 1 GK.

can be observed. Within the experimental uncertainties, the reaction rates are in good agreement.

With this work, the reaction rate is put on a firm experimental basis. The ^{30}S(p,γ) reaction rate is dominated by proton capture into the first low-lying state in ^{31}Cl, see Fig. 8. Missing unambiguous experimental confirmation of this (*tentative*) state prevented a realistic prediction of the reaction rate so far. With this measurement, this uncertainty in the reaction rate has been eliminated. However, because of the limited resolution of the used experimental approach in this work in combination with the AME2012 Q-value uncertainty of 50 keV, the accuracy of the reaction rate in comparison to the reaction rate derived by Wrede *et al.* could not be improved. Table II summarizes the different contributions to the reaction rate under typical rp-process temperatures.

V. SUMMARY

In this work, a Coulomb-breakup experiment of proton-rich ^{31}Cl was used to investigate the low-lying level structure of ^{31}Cl, in order to constrain the important ^{30}S$(p,\gamma)^{31}$Cl bottleneck reaction rate under typical Type I x-ray burst conditions. For the first time, both low-lying proton-decaying states above the particle threshold of $S_p = 296(50)$ keV have been unambiguously identified in one experiment. A low-lying level at an excitation energy of $E_x = 782(32)$ keV has been observed. Theoretical investigations [13] suggest that this is a $J^\pi = 1/2^+$ state. A second level above the proton separation energy at an energy of $E_x = 1793(26)$ keV was observed; here [13] suggests $J^\pi = 5/2^+$.

With this work, the uncertain observation of the astrophysically important first excited state in ^{31}Cl from [11] can now be confirmed experimentally for the first time. Previously, the evidence for this state was only weak. Since proton capture into this state, however, is the dominant contribution in the astrophysical reaction rate under x-ray burst conditions, the confirmation of this particular state is important for further constraints of the ^{30}S$(p,\gamma)^{31}$Cl reaction rate. Moreover, the excitation energy of the second excited state was also observed

TABLE II. The thermonuclear reaction rate for $^{30}S(p,\gamma)^{31}Cl$ for typical rp-process temperatures. The units are $cm^3 mole^{-1} s^{-1}$. The different contributions to the reaction rate are shown (the column with the J^π denotes the resonant capture into the particular state in ^{31}Cl, DC is the direct-capture component, and SUM is the sum of all contributions with the LOW and HIGH uncertainty limits).

T_9 [GK]	DC	$J^\pi = 1/2^+$	$J^\pi = 5/2^+$	SUM	LOW	HIGH
0.08	7.04×10^{-19}	1.48×10^{-27}	8.39×10^{-91}	7.04×10^{-19}	3.52×10^{-19}	1.41×10^{-18}
0.09	7.06×10^{-18}	3.13×10^{-24}	2.12×10^{-80}	7.06×10^{-18}	3.53×10^{-18}	1.42×10^{-17}
0.10	5.14×10^{-17}	1.41×10^{-21}	4.37×10^{-72}	5.14×10^{-17}	2.57×10^{-17}	1.22×10^{-16}
0.14	1.83×10^{-14}	8.47×10^{-15}	9.51×10^{-51}	2.68×10^{-14}	9.16×10^{-15}	7.61×10^{-12}
0.18	9.61×10^{-13}	4.49×10^{-11}	6.17×10^{-39}	4.59×10^{-11}	7.33×10^{-13}	8.86×10^{-09}
0.20	4.58×10^{-12}	8.80×10^{-10}	8.19×10^{-35}	8.85×10^{-10}	1.06×10^{-11}	1.02×10^{-07}
0.24	5.98×10^{-11}	7.36×10^{-08}	1.21×10^{-28}	7.37×10^{-08}	1.54×10^{-09}	3.87×10^{-06}
0.28	4.63×10^{-10}	1.68×10^{-06}	2.97×10^{-24}	1.68×10^{-06}	6.02×10^{-08}	5.01×10^{-05}
0.30	1.12×10^{-09}	5.79×10^{-06}	1.67×10^{-22}	5.79×10^{-06}	2.59×10^{-07}	1.38×10^{-04}
0.34	5.24×10^{-09}	4.38×10^{-05}	1.26×10^{-19}	4.38×10^{-05}	2.82×10^{-06}	7.18×10^{-04}
0.38	1.96×10^{-08}	2.13×10^{-04}	2.31×10^{-17}	2.13×10^{-04}	1.83×10^{-05}	2.60×10^{-03}
0.40	3.53×10^{-08}	4.14×10^{-04}	2.11×10^{-16}	4.14×10^{-04}	4.02×10^{-05}	4.45×10^{-03}
0.44	1.03×10^{-07}	1.29×10^{-03}	9.47×10^{-15}	1.29×10^{-03}	1.55×10^{-04}	1.12×10^{-02}
0.48	2.65×10^{-07}	3.30×10^{-03}	2.23×10^{-13}	3.30×10^{-03}	4.73×10^{-04}	2.39×10^{-02}
0.50	4.08×10^{-07}	4.97×10^{-03}	8.93×10^{-13}	4.97×10^{-03}	7.69×10^{-04}	3.32×10^{-02}
0.54	9.09×10^{-07}	1.02×10^{-02}	1.04×10^{-11}	1.02×10^{-02}	1.81×10^{-03}	5.93×10^{-02}
0.58	1.87×10^{-06}	1.88×10^{-02}	8.62×10^{-11}	1.88×10^{-02}	3.77×10^{-03}	9.70×10^{-02}
0.60	2.62×10^{-06}	2.48×10^{-02}	2.22×10^{-10}	2.48×10^{-02}	5.23×10^{-03}	1.21×10^{-01}
0.64	4.93×10^{-06}	4.04×10^{-02}	1.23×10^{-09}	4.04×10^{-02}	9.42×10^{-03}	1.78×10^{-01}
0.68	8.80×10^{-06}	6.20×10^{-02}	5.56×10^{-09}	6.20×10^{-02}	1.57×10^{-02}	2.51×10^{-01}
0.70	1.16×10^{-05}	7.52×10^{-02}	1.10×10^{-08}	7.52×10^{-02}	1.99×10^{-02}	2.92×10^{-01}
0.74	1.93×10^{-05}	1.07×10^{-01}	3.89×10^{-08}	1.07×10^{-01}	3.04×10^{-02}	3.86×10^{-01}
0.78	3.12×10^{-05}	1.46×10^{-01}	1.20×10^{-07}	1.46×10^{-01}	4.42×10^{-02}	4.94×10^{-01}
0.80	3.91×10^{-05}	1.69×10^{-01}	2.01×10^{-07}	1.69×10^{-01}	5.26×10^{-02}	5.53×10^{-01}
0.84	6.02×10^{-05}	2.19×10^{-01}	5.26×10^{-07}	2.19×10^{-01}	7.23×10^{-02}	6.79×10^{-01}
0.88	9.01×10^{-05}	2.77×10^{-01}	1.26×10^{-06}	2.77×10^{-01}	9.62×10^{-02}	8.16×10^{-01}
0.90	1.09×10^{-04}	3.09×10^{-01}	1.88×10^{-06}	3.09×10^{-01}	1.10×10^{-01}	8.89×10^{-01}
0.94	1.58×10^{-04}	3.78×10^{-01}	4.01×10^{-06}	3.78×10^{-01}	1.40×10^{-01}	1.04×10^{0}
0.98	2.24×10^{-04}	4.54×10^{-01}	8.01×10^{-06}	4.54×10^{-01}	1.75×10^{-01}	1.20×10^{0}
1.00	2.64×10^{-04}	4.94×10^{-01}	1.11×10^{-05}	4.94×10^{-01}	1.95×10^{-01}	1.28×10^{0}
1.20	1.13×10^{-03}	9.62×10^{-01}	1.52×10^{-04}	9.64×10^{-01}	4.43×10^{-01}	2.12×10^{0}
1.40	3.58×10^{-03}	1.49×10^{0}	9.57×10^{-04}	1.50×10^{0}	7.70×10^{-01}	2.95×10^{0}
1.60	9.26×10^{-03}	2.02×10^{0}	3.69×10^{-03}	2.04×10^{0}	1.14×10^{0}	3.69×10^{0}
1.80	2.06×10^{-02}	2.51×10^{0}	1.03×10^{-02}	2.54×10^{0}	1.51×10^{0}	4.31×10^{0}
2.00	4.10×10^{-02}	2.93×10^{0}	2.32×10^{-02}	2.99×10^{0}	1.87×10^{0}	4.82×10^{0}

experimentally, confirming the previously known excitation energy from [11].

Within the error limits, comparison of the extracted excitation energies with the recent IMME calculation and shell-model predictions using the USDB Hamiltonian shows good agreement. The measurement presented in this work is also in good agreement with a similar experiment performed at RIKEN [37].

Furthermore, the thermonuclear reaction rate for the proton-capture reaction on ^{30}S was calculated using spectroscopic information from [13] along with the measured excitation energies from this work. It was also compared to the commonly suggested reaction rate by Wrede *et al.* In general, good agreement is achieved; however, deviations in the excitation energies of the first excited state are reflected in the reaction-rate ratio at temperatures below 1 GK.

ACKNOWLEDGMENTS

The authors want to thank Y. Togano and C. Wrede for helpful discussions. This work was supported by HGF Young Investigators Project No. VH-NG-327, the BMBF under Contracts No. 05P12RDFN8, 06MZ222I, 06MT9156, and 05P12WOFNF, the Alliance Program of the Helmholtz Association (HA216/EMMI), HIC for FAIR, GSI, and the EuroGenesis project MASCHE.

[1] H. Schatz, A. Aprahamian, J. Görres, M. Wiescher, T. Rauscher, J. Rembges, F.-K. Thielemann, B. Pfeiffer, P. Möller, K.-L. Kratz *et al.*, Phys. Rep. **294**, 167 (1998).

[2] H. Schatz, A. Aprahamian, V. Barnard, L. Bildsten, A. Cumming, M. Ouellette, T. Rauscher, F.-K. Thielemann, and M. Wiescher, Phys. Rev. Lett. **86**, 3471 (2001).

[3] J. L. Fisker, H. Schatz, and F.-K. Thielemann, Astrophys. J. Suppl. Ser. **174**, 261 (2008).
[4] H. Schatz and K. Rehm, Nucl. Phys. A **777**, 601 (2006).
[5] D. K. Galloway, M. P. Muno, J. M. Hartman, D. Psaltis, and D. Chakrabarty, Astrophys. J. Suppl. Ser. **179**, 360 (2008).
[6] H. Schatz, L. Bildsten, A. Cumming, and M. Wiescher, Astrophys. J. **524**, 1014 (1999).
[7] W. A. Richter and B. A. Brown, Prog. Theor. Phys. Suppl. **196**, 340 (2012).
[8] M. Wang, G. Audi, A. Wapstra, F. Kondev, M. MacCormick, X. Xu, and B. Pfeiffer, Chin. Phys. C **36**, 1603 (2012).
[9] C. M. Deibel, K. E. Rehm, J. M. Figueira, J. P. Greene, C. L. Jiang, B. P. Kay, H. Y. Lee, J. C. Lighthall, S. T. Marley, R. C. Pardo *et al.*, Phys. Rev. C **84**, 045802 (2011).
[10] G. M. Fuller, W. A. Fowler, and M. J. Newman, Astrophys. J. **252**, 715 (1982).
[11] L. Axelsson, J. Äystö, M. Borge, L. Fraile, H. Fynbo, A. Honkanen, P. Hornshøj, A. Jokinen, B. Jonson, P. Lipas *et al.*, Nucl. Phys. A **634**, 475 (1998).
[12] H. Fynbo, M. Borge, L. Axelsson, J. Äystö, U. Bergmann, L. Fraile, A. Honkanen, P. Hornshøj, Y. Jading, A. Jokinen *et al.*, Nucl. Phys. A **677**, 38 (2000).
[13] C. Wrede, J. A. Caggiano, J. A. Clark, C. M. Deibel, A. Parikh, and P. D. Parker, Phys. Rev. C **79**, 045808 (2009).
[14] C. Iliadis, R. Longland, A. Champagne, A. Coc, and R. Fitzgerald, Nucl. Phys. A **841**, 31 (2010).
[15] C. A. Bertulani and G. Baur, Phys. Rep. **163**, 299 (1988).
[16] G. Baur, C. Bertulani, and H. Rebel, Nucl. Phys. A **458**, 188 (1986).
[17] T. Aumann, Eur. Phys. J A: Hadrons and Nuclei **26**, 441 (2005).
[18] P. Adrich, A. Klimkiewicz, M. Fallot, K. Boretzky, T. Aumann, D. Cortina-Gil, U. Datta Pramanik, T. W. Elze, H. Emling, H. Geissel *et al.* (LAND-FRS Collaboration), Phys. Rev. Lett. **95**, 132501 (2005).
[19] A. Klimkiewicz, N. Paar, P. Adrich, M. Fallot, K. Boretzky, T. Aumann, D. Cortina-Gil, U. Datta Pramanik, T. W. Elze, H. Emling *et al.* (LAND Collaboration), Phys. Rev. C **76**, 051603(R) (2007).
[20] U. D. Pramanik, T. Aumann, K. Boretzky, B. Carlson, D. Cortina, T. Elze, H. Emling, H. Geissel, A. Grünschloß, M. Hellström *et al.*, Phys. Lett. B **551**, 63 (2003).
[21] N. Paar, D. Vretenar, and P. Ring, Phys. Rev. Lett. **94**, 182501 (2005).
[22] R. H. Cyburt, A. M. Amthor, R. Ferguson, Z. Meisel, K. Smith, S. Warren, A. Heger, R. D. Hoffman, T. Rauscher, A. Sakharuk *et al.*, Astrophys. J. Suppl. Ser. **189**, 240 (2010).
[23] http://www.gsi.de/r3b.
[24] H. Geissel, P. Armbruster, K. Behr, A. Bräunle, K. Burkard, M. Chen, H. Folger, B. Franczak, H. Keller, O. Klepper *et al.*, Nucl. Instrum. Methods Phys. Res. B **70**, 286 (1992).
[25] H. Weick, A. H. Sørensen, H. Geissel, C. Scheidenberger, F. Attallah, V. Chichkine, S. Elisseev, M. Hausmann, H. Irnich, Y. Litvinov *et al.*, Nucl. Instrum. Methods Phys. Res. B **193**, 1 (2002).
[26] V. Metag, D. Habs, K. Helmer, U. v. Helmolt, H. Heyng, B. Kolb, D. Pelte, D. Schwalm, W. Hennerici, H. Hennrich *et al.*, *Detectors in Heavy-Ion Reactions* (Springer, Berlin/Heidelberg, 1983), Vol. 178 of Lecture Notes in Physics, pp. 163–178.
[27] J. Alcaraz, B. Alpat, G. Ambrosi, P. Azzarello, R. Battiston, B. Bertucci, J. Bolmont, M. Bourquin, W. Burger, M. Capell *et al.*, Nucl. Instrum. Methods Phys. Res. A **593**, 376 (2008).
[28] J. Cub, G. Stengel, A. Grünschloß, K. Boretzky, T. Aumann, W. Dostal, B. Eberlein, T. Elze, H. Emling, G. Ickert *et al.*, Nucl. Instrum. Methods Phys. Res. A **402**, 67 (1998).
[29] K. Mahata, H. Johansson, S. Paschalis, H. Simon, and T. Aumann, Nucl. Instrum. Methods Phys. Res. A **608**, 331 (2009).
[30] http://fairroot.gsi.de/
[31] K. Boretzky, A. Grünschloß, S. Ilievski, P. Adrich, T. Aumann, C. A. Bertulani, J. Cub, W. Dostal, B. Eberlein, T. W. Elze *et al.* (LAND Collaboration), Phys. Rev. C **68**, 024317 (2003).
[32] K. Setoodehnia, A. A. Chen, J. Chen, J. A. Clark, C. M. Deibel, S. D. Geraedts, D. Kahl, P. D. Parker, D. Seiler, and C. Wrede, Phys. Rev. C **82**, 022801(R) (2010).
[33] B. A. Brown and W. A. Richter, Phys. Rev. C **74**, 034315 (2006).
[34] B. A. Brown, W. D. M. Rae, E. McDonald, and M. Horoi, NUSHELLX@MSU, http://www.nscl.msu.edu/~brown/resources/resources.html
[35] C. Iliadis, *Nuclear Physics of Stars*, Physics Textbook (Wiley-VCH, Weinheim, 2007).
[36] H. Herndl, J. Görres, M. Wiescher, B. A. Brown, and L. Van Wormer, Phys. Rev. C **52**, 1078 (1995).
[37] Y. Togano, T. Motobayashi, N. Aoi, H. Baba, S. Bishop, X. Cai, P. Doornenbal, D. Fang, T. Furukawa, K. Ieki *et al.*, J. Phys. Conf. Ser. **312**, 042025 (2011).